

Reduction and Photoreduction of NO₂ in Humic Acid Films as a Source of HONO, ClNO, N₂O, NO_x, and Organic Nitrogen

Heather M. Ricker, Angelina Leonardi, and Juan G. Navea*

Cite This: *ACS Earth Space Chem.* 2022, 6, 3066–3077

Read Online

ACCESS |



Metrics & More



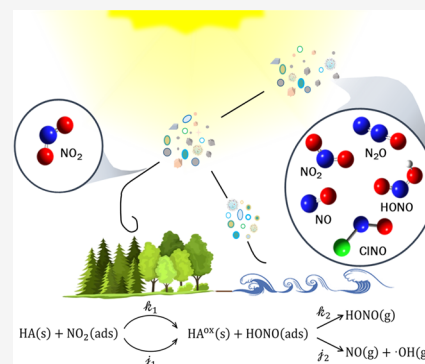
Article Recommendations



Supporting Information

ABSTRACT: Atmospheric nitrous acid (HONO), a trace atmospheric gas, is often underestimated in global atmospheric models due to the poor understanding of its daytime sources and sinks. HONO is known to accumulate during nighttime and undergo rapid photodissociation during the day to form NO and highly reactive OH radical, making it important to have accurate atmospheric HONO estimations. Despite its rapid photolysis, recent field observations have found quasi-steady-state concentrations of HONO at midday, suggesting photolytic HONO formation pathways to replenish daytime atmospheric HONO. Recent studies suggest that the presence of complex organic photosensitizers in atmospheric aerosols converts atmospheric NO₂ into HONO. To better understand the effect of environmental photosensitizers in daytime mechanisms of HONO formation, we present here laboratory studies on the heterogeneous photolytic reduction of NO₂ by humic acid films, a proxy for organic chromophoric compounds. The effect of pH and Cl[−] in the photosensitized formation of HONO and other nitrogen-containing gases is also investigated. A dual Fourier transform infrared (FTIR) system is utilized to simultaneously perform in situ analysis of condensed-phase reactants and gas-phase products. We find that the rate of HONO formation is faster at lower pHs. Nitrogen incorporation in the complex organic chromophore is observed, suggesting a competing pathway that results in suppressed daytime formation of nitrogenous gases. Significantly, the presence of chloride ions also leads to the organic-mediated photolytic formation of nitrosyl chloride (ClNO), a known precursor of HONO. Overall, this work shows that organic acid photosensitizers can reduce adsorbed NO₂ to form HONO, ClNO, and NO while simultaneously incorporating nitrogen into the organic chromophores present in aerosol.

KEYWORDS: photosensitization, sea spray, aerosols, photochemistry, nitrous acid, N-containing organics, nitrosyl chloride



1. INTRODUCTION

Daytime photolysis of nitrous acid (HONO) at wavelengths between 300 and 400 nm has been recognized as a major source of tropospheric hydroxyl radical (OH) in the atmospheric boundary layer (reaction 1),^{1,2} with recent studies suggesting that HONO photodissociation accounts for 30–60% of tropospheric OH radicals, a key atmospheric oxidizer.^{3–5}



Hydroxyl radical, such as those formed by reaction 1, is an important oxidizing agent in the atmosphere, leading to secondary particle formation and determining the lifetime of most trace gases in the atmosphere.^{6–13} Yet, despite the importance of HONO as a precursor of OH radicals, current HONO formation mechanisms underestimate its concentration in the troposphere.^{14–16}

Over the last decades, several studies have shown that HONO accumulates during nighttime through different mechanisms, mainly through direct emissions and heterogeneous nitrate and NO₂ reduction in soil and minerals, photodissociating at early hours of the day.¹⁷ Despite its

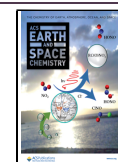
relatively rapid photolysis, recent studies have found a quasi-steady-state concentration of HONO at the daytime. These studies have shown midday maximum concentrations of HONO in rural,^{18–20} urban,^{4,20,21} and marine environments,^{22,23} with values near 0.110, 0.7–1, and 5–10 pptv, respectively. Such observations suggest an unaccounted photolytic source of HONO. In fact, recent works have shown that HONO can be generated via photolysis of surface-bound nitrate,^{11,24–26} and by the reduction of nitrates in the mineral dust deliquescent layer.^{17,27} More recently, HONO has been found to form through the photosensitization of nitrates and humid NO₂, using humic substances, marine-derived organic chromophores, and molecular model systems as photosensitizers.^{5,27–30} The NO₂ background concentrations in remote marine and rural locations are the result of

Received: September 12, 2022

Revised: November 18, 2022

Accepted: November 21, 2022

Published: December 1, 2022



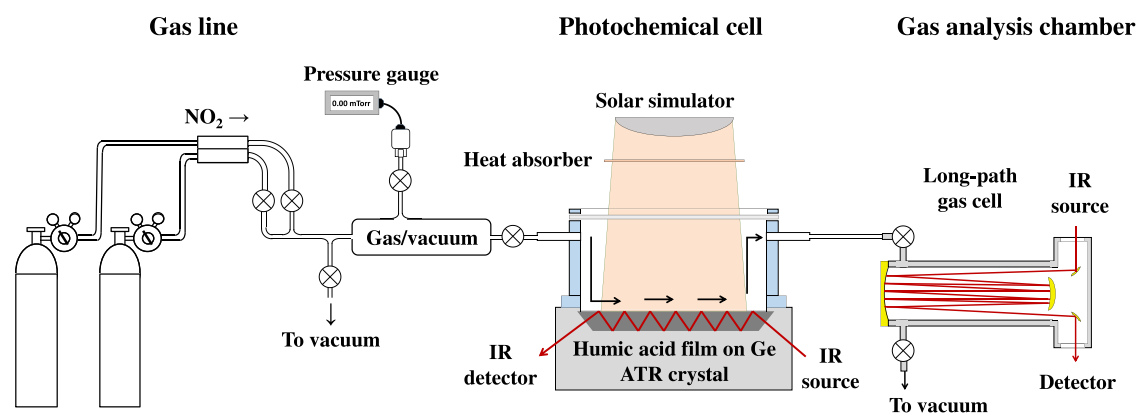


Figure 1. Experimental setup diagram consisting of three segments: Gas line allows for the controlled introduction of NO_2 . Photochemistry and condensed-phase analysis takes place in the photochemical cell, while nitrogenous products are simultaneously analyzed in the gas analysis chamber.

biogenic processes, with higher concentrations ($\sim 1.0 \times 10^{16}$ molecules cm^{-2}) resulting from anthropogenic emissions. Environmental aspects such as the role of chloride ions (Cl^-) and pH continue to be an open question in the photosensitized formation of HONO from NO_2 .

Photosensitizers contained within humic acids (HA) and marine-chromophoric dissolved organic matter (m-CDOM) are macromolecular organic compounds derived from the degradation of biological materials.^{31–35} These chromophores have been observed to partition into atmospheric aerosols, suspensions of liquid or solid particles in the atmosphere with a wide variety of composition, and a highly acidic deliquescent layer. Photosensitizers contained within these aerosol particles are, therefore, in a highly acidic media ($\text{pH} \approx 1–3$).³⁶ The aromatic and carboxylic groups contained in humic substances absorb light in the UV region of the spectrum (up to 400 nm) well within the atmospheric cutoff of solar radiation, making them potential environmental photosensitizers.^{34–37} In addition, it has been found that HA uptake of NO_2 increases at the daytime, through the absorption of solar radiation,^{38–40} suggesting that solar radiation increases the organic chromophore– NO_2 interaction and potential photosensitization of NO_2 . The functional groups in HA are also known reducing agents, a critical property in the potential conversion of NO_2 into HONO and other reduced nitrogenous gases.³¹ In particular, the photosensitizing ability of m-CDOM within sea spray aerosols (SSA), one of the most abundant forms of natural atmospheric aerosols, has been well established, but it is also a highly complex system that can become highly concentrated in submicrometer SSA particles.^{34,41,42} The role of organic chromophores can have a significant impact on the chemical balance of the lower atmosphere and their physical and chemical properties can change based on their environmental conditions. For instance, organic-containing photosensitizers within sea spray aerosols are more likely to contain higher concentrations of chloride ions than their terrestrial counterparts.

The ability of complex organic acids to absorb light changes as a function of environmental parameters, such as ionic species around the chromophore and pH-driven speciation of the organic acid.⁴¹ Recent work has shown that protonated and deprotonated species can not only change the physicochemical nature of the interaction between organic film and substrate but also the properties of the chromophore.⁴² Specifically, pH can affect the wavelength and the relative absorbance intensity

of the photosensitizers.⁴¹ Similarly, the presence of chloride ions (Cl^-) can lead to structural changes that affect the adsorption of NO_2 by the organic material and the light absorption of the chromophore.⁴¹ The presence of Cl^- in the heterogeneous chemistry and photochemistry on tropospheric mineral aerosol or liquid droplets has been shown to produce chlorine-active gaseous product species (Cl_2 , ClNO , ClNO_2 , etc.).^{43–47} The significance of these chlorinated gases on atmospheric processes such as the Antarctic ozone depletion has been well established.^{48–51} In addition, species such as nitrosyl chloride (ClNO), a thermal precursor of HONO, have been proposed to be formed in the troposphere, from the marine boundary layer to terrestrial environments, where it photolyzes quickly to form Cl radicals or hydrolyzes to form HONO.^{43,47,52,53} Yet, the ClNO formation mechanisms involving the conversion of the ubiquitous Cl^- are poorly understood and have not been investigated in the context of heterogeneous photochemistry involving organic chromophores.

In this work, the daytime conversion of NO_2 by HA into nitrogenous gases, including HONO and ClNO , is investigated at atmospherically relevant pHs of 1.5 and 4.5. To better understand the effect of Cl^- in the photochemistry of NO_2 adsorbed on HA, reactions were carried out in the presence and absence of Cl^- at both pHs investigated. In addition, we report changes in the HA photosensitizer as a result of exposure to NO_2 during the photoinduced reaction, a process that sheds light on the aging of organic chromophores in the atmosphere.

2. EXPERIMENTAL SECTION

2.1. In Situ FTIR Spectroscopy of the Heterogeneous Conversion of NO_2 . The experimental setup and protocol are adapted from a previously described work.^{24,25} Photochemical reactions were carried out in a two-part apparatus consisting of a photochemical cell containing the NO_2 -treated humic acid film and a long-path cell measuring the gas-phase products that arise from the irradiation of the condensed phase (Figure 1). Reactions took place on a $72 \times 4 \text{ mm}^2$ horizontal attenuated total reflection (ATR) germanium crystal (PIKE Technologies) enclosed in a 54.0 cm^3 Teflon cell equipped with a UV-transmission window (Ultran) on top that filters light of wavelengths below 290 nm. A thin film of the HA reactant was deposited homogeneously on the ATR crystal, allowing for the monitoring of changes in the HA reactant. The Teflon cell has

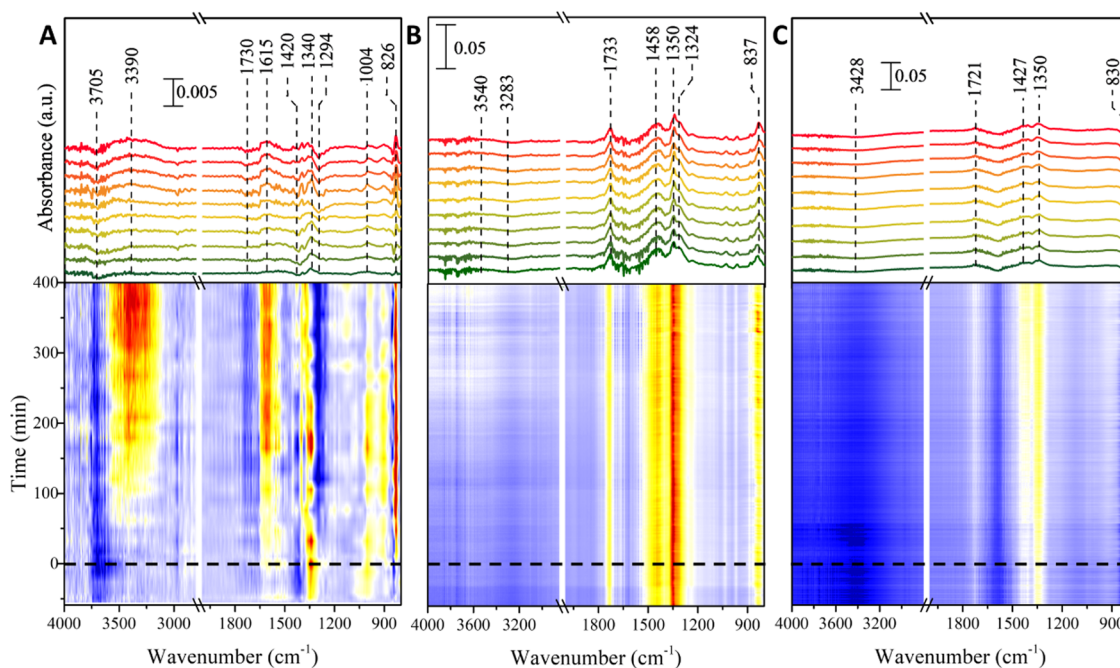


Figure 2. HA film prepared with (A) water, for a pH of 4.5; (B) HCl, for a pH of 1.5; and (C) NaCl, for a pH of 4.5. Top panels: representative vibrational spectra of humic acid thin film after NO_2 treatment, with time increasing from bottom green to top red. The first two FTIR scans are from before irradiation begins, followed by a scan from 5 min after irradiation and subsequent scans with ~ 60 min intervals. Bottom panels: time-gradient of spectral peak intensity, with dark blue being the lowest relative intensity and red being the highest relative intensity. The dashed line at $t = 0$ min indicates when irradiation began.

a gas inlet that connects to the vacuum and NO_2 lines, so the HA thin film can be exposed to known pressures of NO_2 . A valve-controlled outlet allows gases to diffuse from the photochemical cell to the long-path gas cell. The volume of tubing connecting the photochemical cell to the vacuum/ NO_2 introduction system to the long-path gas cell is considered negligible. A broadband ($\lambda > 300$ nm) xenon solar simulator (Newport) with an average output of 120 mW/cm^2 , roughly equivalent to one solar constant at sea level, is positioned above the photochemical cell; a heat absorber window removes infrared radiation to ensure isothermal 298 K reaction conditions. The IR long-path cell (Pike Technologies) is a 100.0 cm^3 cell with a 2.4 m optical path length, equipped with barium fluoride (BaF_2) windows and gold-coated optics. This long-path cell allows for low concentrations of gaseous products to be detected and quantified outside the region of irradiation. The photochemical cell and the long-path gas cell are each connected to Fourier-transformed infrared (FTIR) spectrometers (Thermo, 6700 and iS50, respectively) for in situ time-dependent data. Infrared scans are recorded under initial vacuum and dark conditions, which allows gaseous products to diffuse to the long-path cell throughout the experiment.²⁵ After an initial 60 min under dark conditions, the broadband light source is turned on to begin the photochemical reaction ($t = 0$ min) for a minimum of 400 min. During irradiation, both the ATR-FTIR spectra of the HA thin film and the concomitant gaseous products are recorded every 44 s at a 4 cm^{-1} resolution.

Commercially available humic acid (HA, Sigma-Aldrich), NO_2 gas (98.0%), hydrochloric acid (HCl, Sigma-Aldrich, 37%), and sodium chloride (NaCl, Sigma-Aldrich) were used in this study. In a typical experiment, about 450 mg of HA was ground using a mortar and pestle and then moistened using $18 \text{ M}\Omega$ water, 3 M HCl solution, or 3 M NaCl solution, to obtain

a slurry. The pH of the HA slurry was measured using double-junction pH electrodes (Orion AquaPro) for accurate pH measurements of viscous thin-layer samples with a minimal amount of water used to prepare the slurry. The sample was deposited onto the ATR crystal as a visually homogeneous thin film and left overnight under a flow of dry air ($\text{RH} < 2\%$) to remove excess water; then the dried sample was placed in the photochemical cell apparatus and left under vacuum overnight. The photochemical cell was isolated from the long-path cell and a known partial pressure of NO_2 was allowed to interact with the HA thin film for a minimum time of 8 h. Typically, 1.5 mbar of NO_2 was adsorbed per every mg of HA thin film before placing the system under vacuum and opening the connection to the long-path gas analysis cell. No uncommon safety hazards were encountered during experiments.

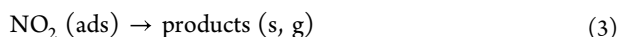
The partial pressures of most gaseous species were determined using a Beer's law calibration using gas standards at 99.9% purity (Sigma-Aldrich) in the long-path cell. The NO absorption cross section in the spectral region between 1973 and 1880 cm^{-1} was determined to be 0.265 Torr^{-1} ; N_2O absorption cross section in the spectral region between 2263 and 2143 cm^{-1} was 6.8164 Torr^{-1} ; and NO_2 absorption cross section in the spectral region between 1660 and 1550 cm^{-1} was 13.177 Torr^{-1} . The partial pressure of HONO and ClNO were determined from previously reported cross sections.^{43,54–56}

3. RESULTS AND DISCUSSION

3.1. Photosensitization of NO_2 –Humic Acid Thin Films. **3.1.1. Vibrational Spectroscopy of Condensed Phase.** Figure 2 shows a time lapse of the vibrational spectroscopy of the photochemical reaction of HA thin film prepared with water, HCl, and NaCl and exposed to NO_2 . The top panel shows spectra from a typical reaction after the humic

acid was treated with NO₂. Of the 10 spectra displayed with time increasing up the figure, the first two scans were taken before irradiation, the third scan was taken after 5 min of irradiation, and the remaining seven scans are spaced by a nearly 60 min interval. Positive bands are attributed to product formation, while negative bands correspond to features that are being lost during irradiation. The bottom panel is a gradient of spectral peak intensity through time, with time increasing on the *y*-axis and the dashed line at time *t* = 0 min notating when daytime conditions were initiated. The intensity gradient shows yellow to red for positive bands and dark blue for negative vibrational bands. All scans are referenced to the HA thin film. Figure 2A,C shows the thin-film reaction progress at pH 4.5 in the absence and presence of Cl⁻, respectively. Figure 2B shows pH 1.5 acidified with HCl as described in Section 2 (vide supra).

Figure 2 shows vibrational bands centered around 826–837 and 1340–1350 cm⁻¹ upon exposure of HA thin films with NO₂, before the broadband light irradiation (below the dashed line in Figure 2). Since the HA thin film is a powder-like complex mixture of precipitated organic oligomers, NO₂ diffusion through the HA sample can lead to adsorption and reactive uptake. These bands are interpreted as a combination of the vibrational stretching and bending modes of adsorbed NO₂ in the HA sample, with symmetric stretching of NO and NO₂ showing at 826–837 and 1340–1350 cm⁻¹, respectively. Simultaneously, gaseous NO₂ is detected in the long-path cell, suggesting that the adsorbed NO₂ is continuously degassing, in agreement with Han et al. observations of adsorption equilibrium of NO₂ in HA thin films, with a fraction of adsorbed NO₂ reacting to form products both in condensed and gas phases^{38,57}

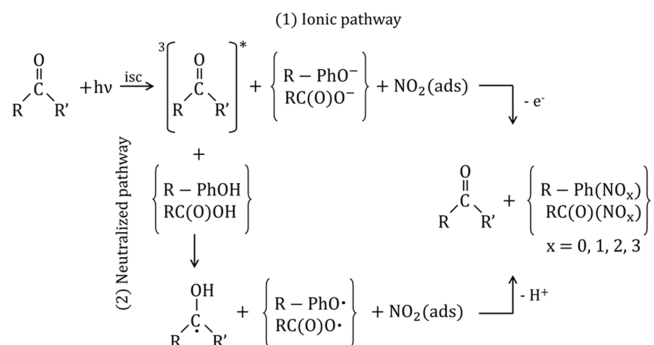


where NO₂(g) and NO₂(ads) represent gaseous and adsorbed NO₂, respectively, with HA film as the adsorbing site. In reaction 3, products are divided into gaseous phase and condensed-phase products, where the latter come from nitrogen incorporation onto the HA thin film.

At the beginning of the experiment, before irradiation, Figure 2A shows a distinctive valley around 3705 cm⁻¹, and a small depression centered at 1420 cm⁻¹. These negative bands correspond to the OH stretch and bending modes, respectively, suggesting that NO₂ is bound primarily through OH groups from phenolic and carboxylic groups of the HA thin film. As mentioned above, positive bands are attributed to the binding of NO₂ and the formation of nitrogen-containing species. Upon irradiation, the peak intensity at 1340 cm⁻¹ undergoes a slight blue shift, matching several stretching modes of nitrates and nitrogen-containing organic compounds. Simultaneously, the growth of a broad band centered around 1615 cm⁻¹, attributed to organo-nitrate asymmetric stretch (R–O–NO₂) can also be seen to grow upon irradiation.^{57,58} The widening peak centered around 1340 cm⁻¹ and the peak at 1420 cm⁻¹ corresponds to a NO stretch, and the peak at 1004 cm⁻¹ corresponds to a C–N stretch.⁵⁹ Further evidence of nitrogen incorporation and changes to the organic film is the decrease in the peak intensities of the carbonyl (C=O) stretch at 1730 cm⁻¹ and the C–O stretch at 1294 cm⁻¹ during irradiation, suggesting that the photo-reactive uptake of NO₂ involves carboxylic acids and phenolic groups. Additionally,

Figure 2A shows an increase in the band centered around 3390 cm⁻¹, which corresponds to OH stretching mode.⁶⁰ These changes suggest that the humic acid thin film was oxidized in the presence of light, as indicated in the ionic or deprotonated pathway in Scheme 1. The presence of chloride ions caused

Scheme 1. Proposed Photoinduced Nitrogen Incorporation Pathways for the Humic Acid Thin Film⁴



⁴R and R' represent arbitrary aromatic substituents in HA. R-PhOH and RC(O)OH represent phenolic and carboxylic acid groups in HA. Charge balance occurs through electron or proton transfer to other parts of the organic. isc = intersystem crossing.

minimal changes in the intensity of any peaks during irradiation, as seen in Figure 2B,C, with the only peak that changed significantly being the growth of the NO stretch from 830 to 837 cm⁻¹. The small but detectable changes, better observed in the heat map in Figure 2, are also observed in the NO stretch region around 1500–1300 cm⁻¹, suggesting that limited photoinduced nitrogen incorporation took place when the humic acid thin film was prepared with chloride ions compared to preparation without chloride ions. The spectral changes described above are the result of photochemical nitrogen incorporation in the HA thin film, initiated by the excitation of the chromophoric components in HA, such as aromatic carbonyl groups, as summarized in Scheme 1.

The initial excitation of the chromophoric components within HA leads to the photosensitization reaction, with some excited chromophoric groups relaxing through energy transfer to other nonchromophoric groups within HA in an intramolecular reaction or via direct photolysis.¹³ As shown in Scheme 1, nitrogen incorporation in the HA thin film depends on the environmental conditions, with two possible mechanisms leading to HA reactive uptake of NO₂: (1) at relatively higher pH (pH 4.5), deprotonated or partially deprotonated species in HA can result in a direct reactive uptake of NO₂, where the conjugate base of the humic acid reacts with adsorbed NO₂; conversely, at lower pH (2) protonated species in HA (pH 1.5) or species neutralized by Na⁺ enhance the reactive uptake of NO₂ by decreasing electrostatic repulsions within the thin film.⁵ The reported pK_as of HA are around 3.0–5.0,^{31,61,62} suggesting that the higher pHs examined in this work correspond to a partially deprotonated HA thin film, opening pathway (1) for the incorporation of nitrogen in the condensed phase. Under these conditions, the deprotonation of phenolic and carboxylic groups within HA favors nitrogen incorporation into the organic thin film as electron donor compounds react thermally with NO₂, an electron acceptor. Broadband radiation enhances this process through photosensitization.³⁸ Alternatively, the chromophoric compounds,

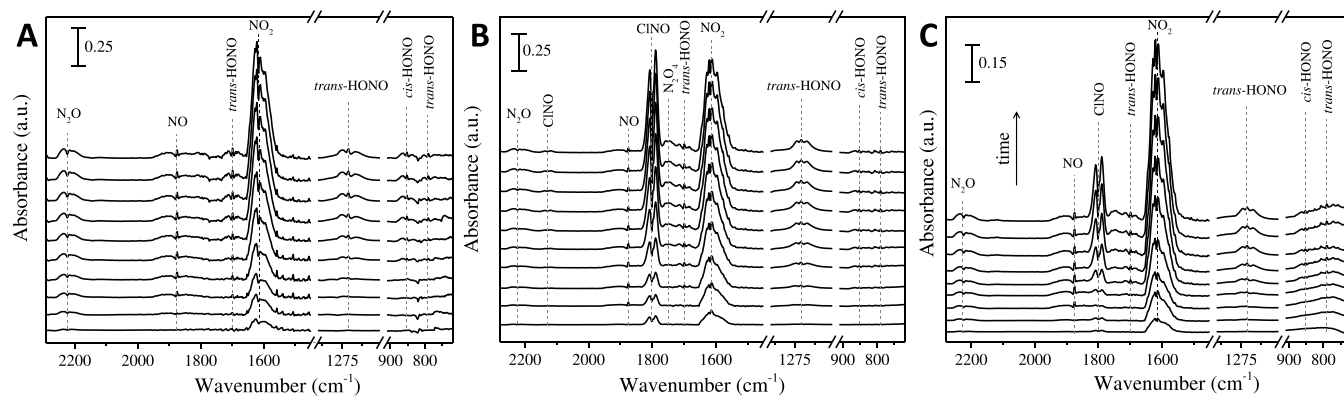


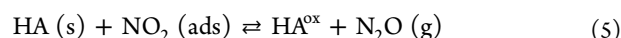
Figure 3. Time progression of gas-phase products—one scan before 60 min and 5 min after irradiation, and subsequent FTIR scans with 60 min intervals. (A) HA film at pH 4.5; (B) HA film at pH 1.5, acidified using HCl; (C) HA film at pH 4.5 with NaCl.

such as aromatic carbonyl groups in HA, produce the excited triplet state in a high quantum yield. This triplet state acts as an electron acceptor and reacts with electron donors, such as phenolic groups. This reaction can lead to the formation of the ketyl radical, which reacts with adsorbed NO_2 (Scheme 1, neutralized pathway). Ultimately, the presence of deprotonated species in pH 4.5 opens both the ionic and neutralized pathways, while pH 1.5 allows only for the protonated path to take place. However, the protonated path leading to nitrogen incorporation in the HA thin film is hindered by parallel reactions leading to gaseous products as well (vide infra).

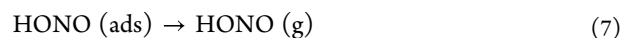
Similarly, the presence of Cl^- hinders nitrogen incorporation in the condensed phase by favoring mechanisms that lead to gaseous products. In the presence of Cl^- , either by the presence of NaCl or by the protonation of HA through the addition of HCl, the HA conjugate base is neutralized, leading NO_2 to heterogeneously react with Cl^- , which competes with reactions involving the organic thin film.⁴³ The addition of Cl^- also increases electrostatic repulsions within the thin film, minimizing reactive nitrogen uptake by HA.⁵ Thus, the presence of Cl^- results in less nitrogen incorporation and the evolution of chlorinated nitrogenous gases.

3.1.2. Vibrational Spectroscopy of Gaseous Products. Figure 3, matching the conditions of the condensed-phase spectra shown in Figure 2, shows representative vibrational spectra of gaseous products in the long-path cell at different stages of the photochemical reaction. Figure 3 represents the time progression of the gas-phase experimental vibrational spectral data, where the 10 spectra displayed correspond to two scans before irradiation, a scan after 5 min of irradiation, and seven subsequent FTIR scans with nearly 60 min intervals.

Figure 3A shows gas products from the irradiation of HA thin film exposed to NO_2 at pH 4.5, in the absence of Cl^- , with the bottom three vibrational spectra corresponding to gaseous products before or just at the beginning of broadband irradiation. The band clearly distinguished at 1616 cm^{-1} , attributed to NO_2 , is continuously growing. Due to the low-pressure conditions of the experiment, adsorbed NO_2 is slowly degassing. In addition, Figure 3A shows a small but distinguishable growth of two bands before irradiation begins, centered at 1878 and 2221 cm^{-1} and attributed to NO and N_2O , respectively. These two gases are thermal products suggesting that the initial reactive uptake of NO_2 with electron donor groups within the HA thin film leads to a dark redox reaction which further changes the chemistry of the HA photosensitizer



where HA behaves as a reducing agent of $\text{NO}_2 (\text{ads})$, producing an oxidized humic acid (HA^{ox}), as shown in reactions 4 and 5. Negligible formation of gaseous HONO is observed thermally at pH 4.5 in the absence of Cl^- . However, the presence of chloride ions causes measurable thermal production of HONO, seen at 1275 cm^{-1} at both pH 1.5 and pH 4.5 (Figure 3B,C). This thermal production follows a similar redox reaction pathway as reactions 4 and 5, where adsorbed NO_2 is reduced to form adsorbed HONO (reaction 6). The presence of Cl^- favors electron transfers in the thermal redox reaction, enhancing the thermal formation of adsorbed HONO.^{30,31,63} The HONO formed in the humic acid film can then partition to the gas phase, a process favored by the low-pressure conditions of the experiment



Thus, the rate of thermal production of gaseous HONO depends on reaction 7, with HONO (ads) as an intermediate

$$\frac{d[\text{HONO (g)}]}{dt} = k_7[\text{HONO (ads)}] \quad (8)$$

where k_7 is the rate constant of reaction 7, the desorption of HONO into gas phase. Here, HONO is assumed to diffuse fast to the long-path cell, making gaseous homogeneous photolysis of HONO negligible within the first 8 h of the experiment.^{24,25} As adsorbed HONO partitions to the gas phase, a steady-state approximation analysis of HONO(ads) leads to a rate expression that depends on adsorbed NO_2 and the rate constant in reaction 6

$$\begin{aligned} \frac{d[\text{HONO (ads)}]}{dt} &= k_6[\text{NO}_2 (\text{ads})] - k_7[\text{HONO (ads)}] \\ &\approx 0 \\ [\text{HONO (ads)}] &= \frac{k_6}{k_7}[\text{NO}_2 (\text{ads})] \end{aligned} \quad (9)$$

$$\therefore \frac{d[\text{HONO (g)}]}{dt} = k_6[\text{NO}_2 (\text{ads})] \quad (10)$$

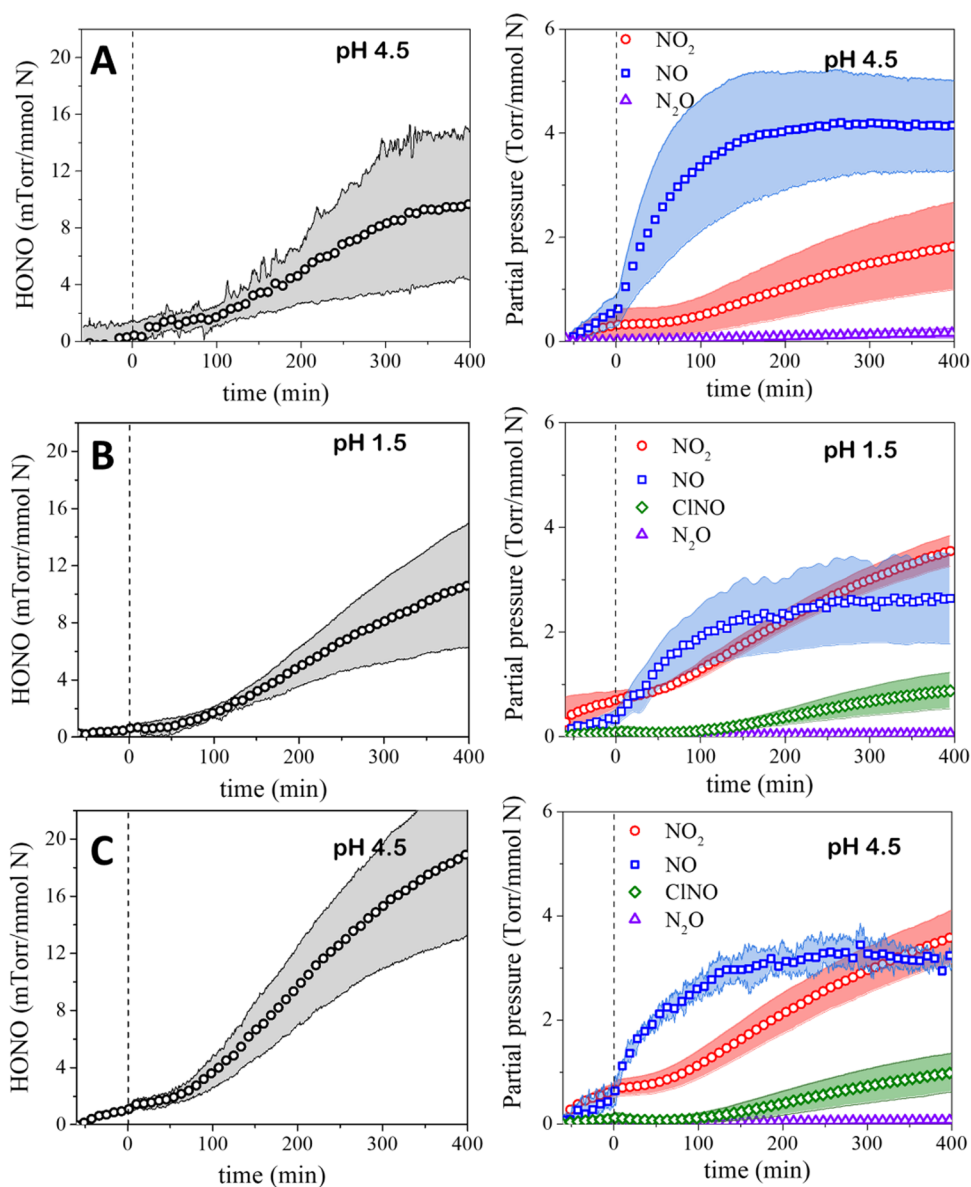


Figure 4. Gas-phase concentrations relative to NO_2 uptake as a function of irradiation of time. (A) Gaseous products at pH 4.5; (B) gaseous products at pH 1.5 acidified with HCl; and (C) gaseous products at pH 4.5 with NaCl. The dashed line at $t = 0$ indicates when irradiation began.

As humic acid active sites are saturated with NO_2 , $[\text{NO}_2(\text{ads})]$ is in large excess and approximately constant, leading to a linear increase in thermal HONO pressures in the presence of chloride ions. This is observed in Figure 4, with a rate constant of HONO formation calculated from the slopes in Figure 4A–C, as $(3.3 \pm 0.5) \times 10^{-6}$, $(6.3 \pm 0.2) \times 10^{-6}$, and $(2.20 \pm 0.02) \times 10^{-5}$ mTorr (mmol N) $^{-1}$ s $^{-1}$, for pH 4.5 (in the absence Cl^-), and pHs 1.5 and 4.5 (in the presence of Cl^-), respectively. Figure 4 shows the time lapse of gaseous products, where $t = 0$ corresponds to the moment when light irradiation over the thin film begins. The ordinates in Figure 4 correspond to the partial pressure of gaseous products, P_{product} in reference to the mmoles of NO_2 adsorbed, $n_{\text{NO}_2(\text{ads})}$, into the HA thin film $\left(\frac{P_{\text{product}}}{n_{\text{NO}_2(\text{ads})}}\right)$.

Once irradiation starts, the rate of formation of NO increases, while the rate of formation of N_2O is not affected (Figure S1), indicating that a light-induced pathway does not exist for N_2O . The photoenhancement effect in the formation

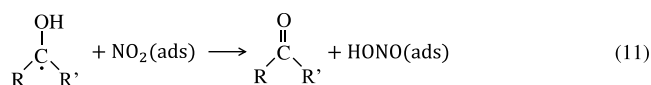
of NO is clearer in Figure 4A–C (right), where there is a linear increase of NO under dark conditions due to the redox reaction (reaction 4), followed by a clear increase in the rate of NO formation at $t = 0$, suggesting a photolytic pathway.

Figure 3A also shows a series of bands growing upon irradiation that are not observed under dark conditions. These bands, centered at 1678, 1262, and 790 cm^{-1} , are attributed to the trans isomer of HONO, while a small but observable band at 852 cm^{-1} is attributed to the cis isomer of HONO. Here, HONO is proposed to be formed through the ketyl radical intermediate formed after HA aromatic carbonyl group excitation (Scheme 1). The ketyl radical reacts with adsorbed NO_2 in a hydrogen transfer reaction to form adsorbed nitrous acid (HONO(ads)), which diffuses to the gas phase because of the acidic pH in the HA thin film and the low-pressure experimental conditions³⁸

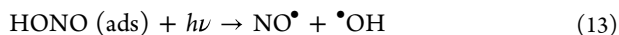
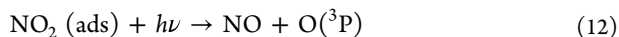
Table 1. Thermal and Thermal + Photochemical Initial Rates of HONO Formation (v_{HONO}) and ClNO (v_{ClNO})^{ab}

pH	v_{HONO} , (mtorr (mmol N) ⁻¹ s ⁻¹) × 10 ⁻⁵	v_{ClNO} , (torr (mmol N) ⁻¹ s ⁻¹) × 10 ⁻⁵	conditions
4.5	0.33 ± 0.05	n.o.	dark
	2.27 ± 0.02	n.o.	light
1.5	0.63 ± 0.02	2.24 ± 0.06	dark, Cl ⁻
	3.20 ± 0.01	4.00 ± 0.02	light, Cl ⁻
4.5	2.20 ± 0.02	2.32 ± 0.02	dark, Cl ⁻
	5.47 ± 0.01	5.50 ± 0.01	light, Cl ⁻

^aDaytime rates correspond to the slope in partial pressure vs time after the QSS period, considered here at 90 min after irradiation. ^bn.o. = not observed.



Reaction 11 is followed by a kinetically controlled desorption with a negligible rate of readsorption of HONO back into the HA thin film (reaction 7). Given the pore diffusion of adsorbed products in the HA thin film,³⁸ it is likely that photosensitive products such as HONO, as well as reactant NO₂, can photodissociate while diffusing through the HA thin film to the headspace of the photochemical cell. This photodissociation leads to the formation of NO, as shown in reactions 1, 12, and 13



where reaction 13 is similar to reaction 1, but taking place on adsorbed HONO and therefore involving a different rate. Both reactions involve the formation of NO, with $\bullet\text{OH}$ and O(³P) known to react with organic species such as those present in the HA thin film.^{11–13,64,65} Thus, consuming OH and O(³P) further displaces reactions 12 and 13 toward products by Le Chatelier's principle.³⁰ Reactions 12 and 13 are, therefore, a source of the NO photoenhancement shown in Figure 4. Ultimately the photosensitized formation of HONO via reaction 11, followed by its diffusion and partition to gas phase, takes place faster than the photodissociation of adsorbed HONO, as indicated by the partial pressure of HONO building up in the long-path cell, as shown in Figure 4A–C (left).

The left panels in Figure 4, showing the partial pressure of HONO (g) with respect to time, show no discernable HONO formation at pH 4.5 under thermal conditions. However, as Cl⁻ are added, there is a clear thermal pathway for HONO formation, with the left panel in Figure 4C showing the most significant HONO formation in the absence of light; this suggests an NO₂ reduction, with HA as the reducing agent (reactions 4, 5, and 6) in the presence of Cl⁻ and deprotonated HA species.^{30,31} Upon irradiation, at pH 4.5 and absence of Cl⁻, Figure 4A shows a light-induced enhancement of HONO formation, following the reaction with the ketyl radical intermediate, as proposed in reaction 11 and shown in Scheme 1. A similar photoenhancement is observed in the formation of HONO in the presence of Cl⁻ and at a more acidic pH. When irradiation begins, thermally generated adsorbed HONO already present in the HA thin film photodissociates to generate NO \bullet and $\bullet\text{OH}$ (reaction 13). This causes a temporary quasi-steady-state (QSS) concentration of HONO (g) until the photosensitized production of HONO builds up enough adsorbed HONO that accumulation in the long-path gas cell is observed. After the QSS period, the partial pressure of HONO

continues to grow, as shown in Figure 4A–C. This effect is also observed for all photoactive gaseous products, including reactant NO₂, as indicated in reactions 12 and 13. Here, the photodissociation of NO₂ and HONO while desorbing from the HA thin film also represents a parallel reaction.

During irradiation, a new steady-state expression for adsorbed HONO is written by combining the thermal and photochemical processes of reactions 6, 7, 11, and 13

$$\begin{aligned} \frac{d[\text{HONO}(\text{ads})]}{dt} &= k_6[\text{NO}_2(\text{ads})] - k_7[\text{HONO}(\text{ads})] \\ &\quad + j_{11}[\text{NO}_2(\text{ads})] \\ &\quad - j_{13}[\text{HONO}(\text{ads})] \\ &\approx 0 \\ [\text{HONO}(\text{ads})] &= \frac{(k_6 + j_{11})}{(k_7 + j_{13})} [\text{NO}_2(\text{ads})] \end{aligned} \quad (14)$$

where j_{11} and j_{13} are the kinetic rate constants for the photochemical reaction (reactions 11 and 13). Substitution of eq 14 into eq 8 yields the rate law expression for HONO formation that combines both thermal and photochemical pathways

$$\frac{d[\text{HONO}(\text{g})]}{dt} = k_7 \frac{(k_6 + j_{11})}{(k_7 + j_{13})} [\text{NO}_2(\text{ads})] \quad (15)$$

Expression 15 is the rate of formation of gaseous HONO in the presence of light. In the absence of a photoenhancement process, $j_{11} = 0$, and eq 15 becomes

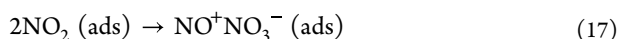
$$\frac{d[\text{HONO}(\text{g})]}{dt} = \frac{k_7 k_6}{(k_7 + j_{13})} [\text{NO}_2(\text{ads})] \quad (16)$$

where eq 16 corresponds to the observed rate of gaseous HONO formation if no photosensitization were taking place. Since $\frac{k_7}{(k_7 + j_{13})} < 1$, $\frac{k_7 k_6}{(k_7 + j_{13})} < k_6$, implying that in the absence of photosensitization, the thermal rate is necessarily larger than that in the presence of light. Yet, in the presence of light, the rate of formation of HONO increases in every experimental condition tested, as shown in Figure 4. This result suggests that $j_{11} \neq 0$ and, therefore, there is a photoenhancement mechanism leading to HONO formation.

As mentioned above, the photoenhancement of HONO production shown in Figure 4 is observed after a QSS period of ~60 to 80 min. After this period, the partial pressure of HONO continues to grow, with the slope of partial pressure of HONO with respect to time (taken after 90 min of irradiation to account for the initial QSS) showing that the rate of

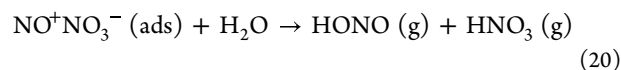
formation of HONO is significantly higher in the presence of light than in the dark (Table 1). Overall, there is an increase in the rate of HONO formation in the presence of light by a factor of 6.9 at pH 4.5 (in the absence of Cl^-), a factor of 5.1 at pH 1.5 (in the presence of Cl^-), and factor of 2.5 at pH 4.5 (in the presence of Cl^-).

Figure 3B,C shows the FTIR spectra of gaseous products in the presence of Cl^- , a ubiquitous ion particularly important in sea spray aerosols (SSA) and in the marine boundary layer (MBL) in general. This figure shows the growth in the absence of light of vibrational bands similar to those observed in Figure 3A: the continuously growing of NO_2 vibrational bands, along with bands assigned to NO and N_2O due to thermal reaction (reactions 4 and 5). A new intense band centered at 1800 cm^{-1} , along with a small but observable band at 2228 cm^{-1} , are attributed to vibrational stretching bands of nitrosyl chloride (CINO). As suggested by the decrease in nitrogen incorporation in the condensed phase in the presence of Cl^- , the neutralization of HA conjugate base leads NO_2 to react with Cl^- via surface-mediated coupling of NO_2 , as proposed by Raff et al. (reaction 17).⁴³ The adsorbed intermediate, NO^+NO_3^- (ads), reacts with Cl^- to form CINO, a labile chlorine compound



The need for dimerization implies that the formation of CINO is either surface-mediated and/or it requires relatively high concentrations of NO_2 in the interface.

Like HONO, CINO is photoactive in the visible region of the spectrum, dissociating into Cl and NO with unit quantum yield (Figure S2).^{66–70} Thus, similar to reactions 12 and 13, the CINO product is initially adsorbed within the HA thin film, and it is likely to photodissociate while diffusing through the organic photosensitizer. Yet, detection and accumulation of CINO in the long-path cell suggests that the rate of formation and diffusion of CINO is faster than its photodissociation under experimental conditions. Thus, CINO formation is also enhanced via photosensitization of NO_2 by HA. Reactions 17 and 18 are competitive reactions that can consume adsorbed NO_2 , decreasing the heterogeneous formation of HONO observed in the absence of Cl^- , as shown in reaction 11, and nitrogen incorporation into the HA film, as described in Scheme 1. The secondary product of reaction 18, NO_3^- , is a well-known chromophore that has been shown to react with HA to form NO_2 and HONO.³⁰ However, relative to the products formed from the adsorption of NO_2 , product yields of NO_3^- are much smaller. Experiments conducted with HA and NO_3^- yielded no measurable products under our experimental conditions. Since CINO has a strong overlap between its absorption cross section and the solar actinic flux, with dissociation quantum yields equal to 1,^{66–70} the proposed mechanism can have important implications in ozone depletion. Significantly, humidity conditions in the atmosphere, leading to water layers on the chromophore particle surface, may also lead to the heterogeneous hydrolysis of CINO or the direct hydrolysis of the adsorbed intermediate, NO^+NO_3^- (ads) to form HONO⁷¹



As a strong electrophile and oxidizing agent, CINO can react with HA as it diffuses toward gaseous phase. In addition, upon photodissociation, Cl^\bullet can also react with the organic thin film resulting in chlorinated organic compounds. However, given the relative amounts of CINO compared to the amount of adsorbed NO_2 , any reaction due to the photolysis of secondary products are minor compared to those resulting from reactions from adsorbed NO_2 . Figure 3B,C also shows a thermal growth of vibrational bands attributed to trans-HONO, suggesting the thermal reduction of NO_2 is enhanced by electrostatic potentials within the thin film due to the presence of Cl^- . This effect can be seen more clearly at higher pH in the presence of NaCl, where the deprotonated fraction of HA and the presence of ions can result in a more effective electron transfer, thereby enhancing the reduction of NO_2 and forming HONO thermally.

As mentioned above, after the initial quasi-steady state, Figure 4 shows that HONO formation is enhanced by light in all three conditions tested, suggesting that reaction 6 takes place faster than any light-induced heterogeneous or homogeneous dissociation of HONO. This pH-dependent photoenhancement is in good agreement with recent studies on photosensitization reactions, showing a light-induced reaction on thin films and aqueous phase where the formation of HONO is faster than photodissociation while diffusing in the matrix.^{5,30} In the absence of thermal mechanisms, there is a slight enhancement in the formation of HONO at lower pH.³⁰ The net direct HONO photoenhancement is higher in the absence of Cl^- , where the rate of formation of HONO increases more than 6 times the rate under dark conditions. Yet, hydrolysis of CINO through reaction 19 can result in significantly higher concentrations of HONO when Cl^- is present in humid conditions. In the presence of Cl^- , a competitive reaction forming CINO results in a relatively lower increase of photoenhancement in HONO formation, compared to that in the absence of light. Importantly, CINO, shown in the right panels of Figure 4B,C, also shows formation in the presence of light, indicating a previously unrecognized heterogeneous photochemical pathway. A decrease in the rate of NO formation is also observed when the rates of photochemical formation of HONO, CINO, and NO_2 are favored over the photodissociation.

Mass balance calculations show that the reactivity of adsorbed NO_2 yields statistically similar formation of nitrogenous gaseous products. Not including desorbed NO_2 as a product, the total yield of gaseous products in each reaction (including both, thermal and photolytic pathways) was (2.4 ± 0.5) , (2.0 ± 0.3) , and $(2.2 \pm 0.1)\%$, for pH 4.5, pH 1.5, and pH 4.5 in the presence of Cl^- , respectively. Percent yield for each gaseous product, as well as desorbed NO_2 , was calculated assuming ideal behavior at minute 400 of irradiation, using eq 21

$$\text{yield} (\%) = \frac{n_{\text{product}}}{n_{\text{NO}_2 (\text{ads})}} \times 100 = \frac{(P_{\text{product}})(V_{\text{GC}})}{RT(n_{\text{NO}_2 (\text{ads})})} \times 100 \quad (21)$$

where n_{product} is the number of moles of nitrogenous gases detected in the long-path cell, V_{GC} is the volume of the long-path cell (100 mL), R is the ideal gas constant, and T is 295 K.

Table 2. Yield (%) of Gaseous Products at 400 min of Irradiation, Considering Both Thermal and Photochemical Products^{ab}

gaseous product	yield (%)		
	pH 4.5	pH 1.5 (Cl ⁻)	pH 4.5 (Cl ⁻)
NO	2.3 ± 0.4(0.3 ± 0.1)	1.4 ± 0.2(0.2 ± 0.1)	1.65 ± 0.03(0.2 ± 0.1)
NO ₂	1.0 ± 0.2(0.2 ± 0.1)	1.92 ± 0.05(0.4 ± 0.1)	2.0 ± 0.1(0.4 ± 0.1)
CINO	n.o. (n.o.)	0.55 ± 0.09(0.06 ± 0.05)	0.5 ± 0.1(0.06 ± 0.05)
HONO	0.006 ± 0.003 (n.o.)	0.007 ± 0.002((30 ± 3) × 10 ⁻⁴)	0.011 ± 0.002((30 ± 3) × 10 ⁻⁴)
N ₂ O	0.10 ± 0.05(0.010 ± 0.008)	0.033 ± 0.008((6 ± 3) × 10 ⁻³)	0.041 ± 0.003((6 ± 3) × 10 ⁻³)

^aValues in parentheses represent the yield after the initial 60 min in the absence of light. ^bn.o.: not observed.

The summary of all of the calculated yields is shown in Table 2.

As Cl⁻ is added to the HA thin film (with H⁺ for pH 1.5 and Na⁺ for pH 4.5), electrostatic repulsions increase, resulting in a larger desorption of NO₂ from HA.⁵ This effect is shown in Figure 4, where the desorption of NO₂ increases as HCl or NaCl is added to the organic thin film. Table 2 shows that the desorption of NO₂ in the absence of light doubles as Cl⁻ is added to the thin film.

The daytime chemistry of NO₂ adsorbed in HA is more complex, as the presence of Cl⁻ can affect not only the gaseous products but also the aerosol phase. The formation of CINO can also impact the atmospheric concentrations of HONO as CINO can hydrolyze to form more HONO, as shown in reaction 11. These laboratory experiments provide evidence that NO₂ can be reduced photolytically by HA. It also shows that relevant environmental factors, such as the presence of ions and pH, result in gaseous products that have not been considered in previous laboratory studies, providing a more holistic picture of the influence of environmental photosensitizers in the atmospheric nitrogen balance.

Overall, HONO formation from NO₂ shown in Figure 4 and Table 2 complements recent work involving surface-mediated processes or photosensitization of NO₂ or nitrates by dissolved organic matter.^{17,24–30,72–76} Daytime formation of HONO via photosensitization of nitrates in solution (0.1 g/mL of humic acids) suggests that organic chromophores can act as photosensitizers.³⁰ In urban regions, where concentrations of NO₂ are likely higher, work with grime has shown that, at high humidity (RH > 50%), polycyclic aromatic hydrocarbons (PAHs) can dissolve in the aerosol deliquescent layer and act as photosensitizers in the conversion of NO₂ into HONO.^{73,75} These recent works have also highlighted the need for a better understanding of the speciation of products in the photochemical reactions leading to HONO formation.⁷² The experiments presented within show previously unrecognized pathways for nitrogenous gases, such as CINO, as well as thermal formation of N₂O, contributing to a more holistic understanding of the speciation of gaseous products in the heterogeneous photochemistry of NO₂ in organic interfaces. In addition to nitrogenous gases, the incorporation of nitrogen into the organic thin film leads to secondary nitrogen-containing species in the condensed phase; this pathway shows similarities with the surface-mediated formation of nitro-organic compounds by the heterogeneous reaction of NO₂ with fatty acids.⁷⁶

4. CONCLUSIONS AND ATMOSPHERIC IMPLICATIONS

The findings shown in this work suggest that the photosensitization of adsorbed NO₂ by humic substances can be a

daytime source of HONO in the troposphere, along with other nitrogenous products. Significantly, the presence of Cl⁻ leads to the photosensitized formation of CINO, a well-known precursor of HONO via hydrolysis. Thus, photosensitization of NO₂ by humic acids can result in a direct pathway for HONO formation or an indirect pathway via intermediary CINO, with the subsequent hydrolysis of CINO to form HONO (reaction 19). In addition, nitrogen incorporation into the complex organic chromophore was observed during irradiation reactions, leading to daytime formation of organic nitrogen compounds in the condensed phase. Yet, this nitrogen incorporation mechanism was hindered in the presence of Cl⁻.

This work provides insights into the sources of HONO and other nitrogenous gases in the troposphere during daytime. Photosensitized reduction of atmospheric NO₂ into HONO and CINO, with HA as a photosensitizer under various atmospherically relevant conditions, including pH and the presence of Cl⁻, has been shown. These results support multiple field observations of HONO in the boundary layer with a peak concentration at noon. The adsorption of NO₂ by aerosols containing HA, as presented here, is one potential way of initiating the formation of HONO and other active nitrogenous gases, such as CINO. These complex environmental chromophores can originate from different sources, including humic substances from natural waters, or marine-chromophoric dissolved organic matter (m-CDOM). The reaction pathways leading to HONO formation involved the formation of a ketyl radical intermediate that is produced upon light absorbance of the chromophore. As the reaction takes place to form gaseous products, nitrogen incorporation can also lead to changes in the chromophore and secondary aerosols, particularly at higher pHs and lower electrostatic potentials, highlighting the importance of environmental conditions in photosensitizing reactions.

Furthermore, there is an important dependence on the presence of chloride ions in the gas-phase products. Organic acids, in the presence of HCl or NaCl from sea salt or various natural or anthropogenic sources, can react with adsorbed NO₂ to form CINO. The reaction pathway is proposed to involve the formation of dimer intermediate NO⁺ NO₃⁻ within the organic thin film. Particularly in polluted regions, where larger emissions of NO₂ can lead to the dimerization required to react with Cl⁻, the formation pathway of CINO can be significant: CINO is the natural reservoir of HONO by hydrolysis that, during daytime, dissociates into NO and highly reactive chlorine atoms. This last reaction is known to initiate secondary reactions with other atmospheric species and can potentially impact the concentration of ozone in the troposphere.

Overall, the findings in this study provide key knowledge regarding the daytime formation of several nitrogenous gases via photosensitization of NO₂ in complex organic interfaces, as

well as the formation of condensed organic nitrogen species. Yet, further consideration concerning the concentration of photosensitizer in the current study should be given with respect to that which occurs in the environment. While this work assumes that the thin films used in our experiments mimic environmental interfacial systems, future work should be conducted to determine how the concentration of photosensitizer affects the formation of HONO and ClNO in aqueous systems.

■ ASSOCIATED CONTENT

SI Supporting Information

The Supporting Information is available free of charge at <https://pubs.acs.org/doi/10.1021/acsearthspacechem.2c00282>.

Gas-phase partial pressure of N₂O relative to NO₂ adsorption and absorbance cross section of photoactive gases detected plotted in comparison to absolute irradiance of the solar simulator and the absorbance of aqueous-phase humic acid (PDF)

■ AUTHOR INFORMATION

Corresponding Author

Juan G. Navea – Chemistry Department, Skidmore College, Saratoga Springs, New York 12866-1632, United States; orcid.org/0000-0002-7723-6033; Email: jnavea@skidmore.edu

Authors

Heather M. Ricker – Chemistry Department, Skidmore College, Saratoga Springs, New York 12866-1632, United States

Angelina Leonardi – Chemistry Department, Skidmore College, Saratoga Springs, New York 12866-1632, United States

Complete contact information is available at: <https://pubs.acs.org/10.1021/acsearthspacechem.2c00282>

Notes

The authors declare no competing financial interest.

■ ACKNOWLEDGMENTS

This work was supported by the National Science Foundation through the 995 NSF Center for Aerosol Impacts on the Chemistry of the Environment, a Center for Chemical Innovation (CHE-1801971). The authors thank Dr. Vicki Grassian, Stephanie Mora-Garcia, and Michael R. Alves for helpful discussions.

■ REFERENCES

- (1) Platt, U. Chemistry of Multiphase Atmospheric. In *The Origin of Nitrous and Nitric Acid in the Atmosphere*; Jaeschke, W., Ed.; Springer: Berlin, 1986; pp 299–319.
- (2) Perner, D.; Platt, U. Detection of nitrous acid in the atmosphere by differential optical absorption. *Geophys. Res. Lett.* **1979**, *6*, 917–920.
- (3) Su, H.; Cheng, Y. F.; Shao, M.; Gao, D. F.; Yu, Z. Y.; Zeng, L. M.; Slanina, J.; Zhang, Y. H.; Wiedensohler, A. Nitrous acid (HONO) and its daytime sources at a rural site during the 2004 PRIDE-PRD experiment in China. *J. Geophys. Res.* **2008**, *113*, No. D14312.
- (4) Ren, X.; Harder, H.; Martinez, M.; Leshner, R. L.; Oligier, A.; Simpas, J. B.; Brune, W. H.; Schwab, J. J.; Demerjian, K. L.; He, Y.; Zhou, X.; Gao, H. OH and HO₂ Chemistry in the urban atmosphere of New York City. *Atmos. Environ.* **2003**, *37*, 3639–3651.
- (5) Han, C.; Yang, W.; Wu, Q.; Yang, H.; Xue, X. Key role of pH in the photochemical conversion of NO₂ to HONO on humic acid. *Atmos. Environ.* **2016**, *142*, 296–302.
- (6) Atkinson, R. Kinetics and mechanisms of the gas-phase reactions of the hydroxyl radical with organic compounds under atmospheric conditions. *Chem. Rev.* **1986**, *86*, 69–201.
- (7) Houle, F. A.; Hingsberg, W. D.; Wilson, K. R. Oxidation of a model alkane aerosol by OH radical: the emergent nature of reactive uptake. *Phys. Chem. Chem. Phys.* **2015**, *17*, 4412–4423.
- (8) George, I. J.; Abbatt, J. P. Heterogeneous oxidation of atmospheric aerosol particles by gas-phase radicals. *Nat. Chem.* **2010**, *2*, 713–722.
- (9) Qiu, C.; Khalizov, A. F.; Zhang, R. Soot aging from OH-initiated oxidation of toluene. *Environ. Sci. Technol.* **2012**, *46*, 9464–9472.
- (10) Kroll, J. H.; Lim, C. Y.; Kessler, S. H.; Wilson, K. R. Heterogeneous Oxidation of Atmospheric Organic Aerosol: Kinetics of Changes to the Amount and Oxidation State of Particle-Phase Organic Carbon. *J. Phys. Chem. A* **2015**, *119*, 10767–10783.
- (11) Leonardi, A.; Ricker, H. M.; Gale, A. G.; Ball, B. T.; Odbadrakh, T. T.; Shields, G. C.; Navea, J. G. Particle formation and surface processes on atmospheric aerosols: A review of applied quantum chemical calculations. *Int. J. Quantum Chem.* **2020**, *120*, No. e26350.
- (12) Gambús, G.; Patiño, P.; Navea, J. Spectroscopic Study of Low-Pressure Water Plasmas and Their Reactions with Liquid Hydrocarbons. *Energy Fuels* **2002**, *16*, 172–176.
- (13) Navea, J. G.; Grassian, V. H. Photochemistry of Atmospheric Particles. In *Reference Module in Chemistry, Molecular Sciences and Chemical Engineering*; Wandelt, K.; Kolasinski, K., Eds.; Elsevier Publishing: Amsterdam, 2017.
- (14) Cui, L.; Li, R.; Zhang, Y.; Meng, Y.; Fu, H.; Chen, J. An observational study of nitrous acid (HONO) in Shanghai, China: The aerosol impact on HONO formation during the haze episodes. *Sci. Total Environ.* **2018**, *630*, 1057–1070.
- (15) Tuite, K.; Thomas, J. L.; Veres, P. R.; Roberts, J. M.; Stevens, P. S.; Griffith, S. M.; Dusanter, S.; Flynn, J. H.; Ahmed, S.; Emmons, L.; Kim, S.; Washenfelder, R.; Young, C.; Tsai, C.; Pikelnya, O.; Stutz, J. Quantifying Nitrous Acid Formation Mechanisms Using Measured Vertical Profiles During the CalNex 2010 Campaign and 1D Column Modeling. *Geophys. Res. Atmos.* **2021**, *126*, No. e2021JD034689.
- (16) Stutz, J.; Alicke, B.; Neftel, A. Nitrous acid formation in the urban atmosphere: Gradient measurements of NO₂ and HONO over grass in Milan, Italy. *J. Geophys. Res.* **2002**, *107*, L0PS-1.
- (17) Kim, D.; Xiao, Y.; Karchere-Sun, R.; Richmond, E.; Ricker, H. M.; Leonardi, A.; Navea, J. G. Atmospheric processing of anthropogenic combustion particles: Iron mobility and nitrite formation from fly ash. *ACS Earth Space Chem.* **2020**, *4*, 750–761.
- (18) Acker, K.; Möller, D.; Wieprecht, W.; Meixner, F. X.; Bohn, B.; Gilge, S.; Plass-Dülmer, C.; Berresheim, H. Strong daytime production of OH from HNO₂ at a rural mountain site. *Geophys. Res. Lett.* **2006**, *33*, No. L02809.
- (19) Kleffmann, J. Ö.; Gavriloaiei, T.; Hofzumahaus, A.; Holland, F.; Koppmann, R.; Rupp, L.; Schlosser, E.; Siese, M.; Wahner, A. Daytime formation of nitrous acid: A major source of OH radicals in a forest. *Geophys. Res. Lett.* **2005**, *32*, No. L05818.
- (20) Kleffmann, J. Ö.; Kurtenbach, R.; Lörzer, J.; Wiesen, P.; Kalthoff, N.; Vogel, B.; Vogel, H. Measured and simulated vertical profiles of nitrous acid—Part I: Field measurements. *Atmos. Environ.* **2003**, *37*, 2949–2955.
- (21) Liu, Y.; Nie, W.; Xu, Z.; Wang, T.; Wang, R.; Li, Y.; Wang, L.; Chi, X.; Ding, A. Semi-quantitative understanding of source contribution to nitrous acid (HONO) based on 1-year of continuous observation at the SORPES station in eastern China. *Atmos. Chem. Phys.* **2019**, *19*, 13289–13308.
- (22) Ye, C.; Zhou, X.; Pu, D.; Stutz, J.; Festa, J.; Spolaor, M.; Tsai, C.; Cantrell, C.; Mauldin, R. L.; Campos, T.; Weinheimer, A.; Hornbrook, R. S.; Apel, E. C.; Guenther, A.; Kaser, L.; Yuan, B.; Karl, T.; Haggerty, J.; Hall, S.; Ullmann, K.; Smith, J. N.; Ortega, J.; Knote,

C. Rapid cycling of reactive nitrogen in the marine boundary layer. *Nature* **2016**, *532*, 489–491.

(23) Kasibhatla, P.; Sherwen, T.; Evans, M. J.; Carpenter, L. J.; Reed, C.; Alexander, B.; Chen, Q.; Sulprizio, M. P.; Lee, J. D.; Read, K. A.; Bloss, W.; Crilley, L. R.; Keene, W. C.; Pszenny, A. A. P.; Hodzic, A. Global impact of nitrate photolysis in sea-salt aerosol on NO_x , OH and O_3 in the marine boundary layer. *Atmos. Chem. Phys.* **2018**, *18*, 11185–11203.

(24) Ostaszewski, C. J.; Stuart, N. M.; Lesko, D. M. B.; Kim, D.; Lueckheide, M. J.; Navea, J. G. Effects of Coadsorbed Water on the Heterogeneous Photochemistry of Nitrates Adsorbed on TiO_2 . *J. Phys. Chem. A* **2018**, *122*, 6360–6371.

(25) Lesko, D. M. B.; Coddens, E. M.; Swomley, H. D.; Welch, R. M.; Borgatta, J.; Navea, J. G. Photochemistry of nitrate chemisorbed on various metal oxide surfaces. *Phys. Chem. Chem. Phys.* **2015**, *17*, 20775–20785.

(26) Nanayakkara, C. E.; Jayaweera, P. M.; Rubasinghege, G.; Baltrusaitis, J.; Grassian, V. H. Surface Photochemistry of Adsorbed Nitrate: The Role of Adsorbed Water in the Formation of Reduced Nitrogen Species on $\alpha\text{-Fe}_2\text{O}_3$ Particle Surfaces. *J. Phys. Chem. A* **2014**, *118*, 158–166.

(27) Scharko, N. K.; Berke, A. E.; Raff, J. D. Release of Nitrous Acid and Nitrogen Dioxide from Nitrate Photolysis in Acidic Aqueous Solutions. *Environ. Sci. Technol.* **2014**, *48*, 11991–12001.

(28) Han, C.; Yang, W.; Yang, H.; Xue, X. Enhanced photochemical conversion of NO_2 to HONO on humic acids in the presence of benzophenone. *Environ. Pollut.* **2017**, *231*, 979–986.

(29) Scharko, N. K.; Martin, E. T.; Losovyj, Y.; Peters, D. G.; Raff, J. D. Evidence for Quinone Redox Chemistry Mediating Daytime and Nighttime NO_2 -to-HONO Conversion on Soil Surfaces. *Environ. Sci. Technol.* **2017**, *51*, 9633–9643.

(30) Garcia, S. L. M.; Pandit, S.; Navea, J. G.; Grassian, V. H. Nitrous Acid (HONO) Formation from the Irradiation of Aqueous Nitrate Solutions in the Presence of Marine Chromophoric Dissolved Organic Matter: Comparison to Other Organic Photosensitizers. *ACS Earth Space Chem.* **2021**, *5*, 3056–3064.

(31) Borgatta, J.; Navea, J. G. Fate of Aqueous Iron Leached from Tropospheric Aerosols during Atmospheric Acidic Processing: Study of the Effect of Humic-Like Substances. *WIT Trans. Ecol. Environ.* **2015**, *198*, 155–166.

(32) Ma, J.; Del Vecchio, R.; Golanoski, K. S.; Boyle, E. S.; Blough, N. V. Optical Properties of Humic Substances and CDOM: Effects of Borohydride Reduction. *Environ. Sci. Technol.* **2010**, *44*, 5395–5402.

(33) Kwon, D.; Sovers, M. J.; Grassian, V. H.; Kleiber, P. D.; Young, M. A. Optical Properties of Humic Material Standards: Solution Phase and Aerosol Measurements. *ACS Earth Space Chem.* **2018**, *2*, 1102–1111.

(34) Trueblood, J. V.; Alves, M. R.; Power, D.; Santander, M. V.; Cochran, R. E.; Prather, K. A.; Grassian, V. H. Shedding Light on Photosensitized Reactions within Marine-Relevant Organic Thin Films. *ACS Earth Space Chem.* **2019**, *3*, 1614–1623.

(35) Trueblood, J. V.; Wang, X.; Or, V. W.; Alves, M. R.; Santander, M. V.; Prather, K. A.; Grassian, V. H. The Old and the New: Aging of Sea Spray Aerosol and Formation of Secondary Marine Aerosol through OH Oxidation Reactions. *ACS Earth Space Chem.* **2019**, *3*, 2307–2314.

(36) Angle, K. J.; Crocker, D. R.; Simpson, R. M. C.; Mayer, K. J.; Garofalo, L. A.; Moore, A. N.; Mora Garcia, S. L.; Or, V. W.; Srinivasan, S.; Farhan, M.; Sauer, J. S.; Lee, C.; Pothier, M. A.; Farmer, D. K.; Martz, T. R.; Bertram, T. H.; Cappa, C. D.; Prather, K. A.; Grassian, V. H. Acidity across the interface from the ocean surface to sea spray aerosol. *Proc. Natl. Acad. Sci. U.S.A.* **2021**, *118*, No. e2018397118.

(37) Luo, M.; Shemesh, D.; Sullivan, M. N.; Alves, M. R.; Song, M.; Gerber, R. B.; Grassian, V. H. Impact of pH and NaCl and CaCl_2 Salts on the Speciation and Photochemistry of Pyruvic Acid in the Aqueous Phase. *J. Phys. Chem. A* **2020**, *124*, 5071–5080.

(38) Han, C.; Yang, W.; Wu, Q.; Yang, H.; Xue, X. Heterogeneous Photochemical Conversion of NO_2 to HONO on the Humic Acid

Surface under Simulated Sunlight. *Environ. Sci. Technol.* **2016**, *50*, 5017–5023.

(39) McNeill, K.; Canonica, S. Triplet state dissolved organic matter in aquatic photochemistry: reaction mechanisms, substrate scope, and photophysical properties. *Environ. Sci.: Processes Impacts* **2016**, *18*, 1381–1399.

(40) Schiffer, J. M.; Mael, L. E.; Prather, K. A.; Amaro, R. E.; Grassian, V. H. Sea Spray Aerosol: Where Marine Biology Meets Atmospheric Chemistry. *ACS Cent. Sci.* **2018**, *4*, 1617–1623.

(41) Karimova, N. V.; Luo, M.; Grassian, V.; Gerber, R. Absorption Spectra of Benzoic Acid in Water at Different pH and in the Presence of Salts: Insights from the Integration of Experimental Data and Theoretical Cluster Models. *Phys. Chem. Chem. Phys.* **2020**, *22*, 5046–5056.

(42) Karimova, N. V.; Luo, M.; Grassian, V. H.; Gerber, R. B. Towards a microscopic model of light absorbing complex organic components in aqueous environments: Theoretical and experimental study. *Phys. Chem. Chem. Phys.* **2021**, *23*, 10487–10497.

(43) Raff, J. D.; Njegic, B.; Chang, W. L.; Gordon, M. S.; Dabdub, D.; Gerber, R. B.; Finlayson-Pitts, B. Chlorine activation indoors and outdoors via surface-mediated reactions of nitrogen oxides with hydrogen chloride. *Proc. Natl. Acad. Sci. U.S.A.* **2009**, *106*, 13647.

(44) Hammerich, A. D.; Finlayson-Pitts, B.; Gerber, R. B. Mechanism for formation of atmospheric Cl atom precursors in the reaction of dinitrogen oxides with HCl/Cl^- on aqueous films. *Phys. Chem. Chem. Phys.* **2015**, *17*, 19360–19370.

(45) Xia, M.; Peng, X.; Wang, W.; Yu, C.; Sun, P.; Li, Y.; Liu, Y.; Xu, Z.; Wang, Z.; Xu, Z.; Nie, W.; Ding, A.; Wang, T. Significant production of ClNO_2 and possible source of Cl_2 from N_2O_5 uptake at a suburban site in eastern China. *Atmos. Chem. Phys.* **2020**, *20*, 6147–6158.

(46) Finlayson-Pitts, B. J. Multiphase chemistry in the troposphere: It all starts ... and ends ... with gases. *Int. J. Chem. Kinet.* **2019**, *51*, 736–752.

(47) Rubasinghege, G.; Grassian, V. H. Surface-Catalyzed Chlorine and Nitrogen Activation: Mechanisms for the Heterogeneous Formation of ClNO , NO , NO_2 , HONO, and N_2O from HNO_3 and HCl on Aluminum Oxide Particle Surfaces. *J. Phys. Chem. A* **2012**, *116*, 5180–5192.

(48) Solomon, S.; Garcia, R. R.; Rowland, F. S.; Wuebbles, D. J. On the depletion of Antarctic ozone. *Nature* **1986**, *321*, 755–758.

(49) Molina, M. J.; Rowland, F. S. Stratospheric sink for chlorofluoromethanes: chlorine atom-catalysed destruction of ozone. *Nature* **1974**, *249*, 810–812.

(50) Barrie, L. A.; Bottenheim, J. W.; Schnell, R. C.; Crutzen, P. J.; Rasmussen, R. A. Ozone destruction and photochemical reactions at polar sunrise in the lower Arctic atmosphere. *Nature* **1988**, *334*, 138–141.

(51) Perner, D.; Arnold, T.; Crowley, J.; Klüpfel, T.; Martinez, M.; Seuwen, R. The Measurement of Active Chlorine in the Atmosphere by Chemical Amplification. *J. Atmos. Chem.* **1999**, *34*, 9–20.

(52) Thornton, J. A.; Kercher, J. P.; Riedel, T. P.; Wagner, N. L.; Cozic, J.; Holloway, J. S.; Dubé, W. P.; Wolfe, G. M.; Quinn, P. K.; Middlebrook, A. M.; Alexander, B.; Brown, S. S. A large atomic chlorine source inferred from mid-continental reactive nitrogen chemistry. *Nature* **2010**, *464*, 271–274.

(53) Karlsson, R. S.; Ljungström, E. B. Laboratory Study of ClNO : Hydrolysis. *Environ. Sci. Technol.* **1996**, *30*, 2008–2013.

(54) Wingen, L. M.; Barney, W. S.; Lakin, M. J.; Brauers, T.; Finlayson-Pitts, B. J. A Unique Method for Laboratory Quantification of Gaseous Nitrous Acid (HONO) Using the Reaction $\text{HONO} + \text{HCl} \rightarrow \text{ClNO} + \text{H}_2\text{O}$. *J. Phys. Chem. A* **2000**, *104*, 329–335.

(55) Barney, W. S.; Wingen, L. M.; Lakin, M. J.; Brauers, T.; Stutz, J.; Finlayson-Pitts, B. J. Infrared Absorption Cross-Section Measurements for Nitrous Acid (HONO) at Room Temperature. *J. Phys. Chem. A* **2000**, *104*, 1692–1699.

(56) Finlayson-Pitts, B. J. Reaction of NO_2 with NaCl and atmospheric implications of NOCl formation. *Nature* **1983**, *306*, 676–677.

- (57) Stemmler, K.; Ammann, M.; Donders, C.; Kleffmann, J.; George, C. Photosensitized reduction of nitrogen dioxide on humic acid as a source of nitrous acid. *Nature* **2006**, *440*, 195.
- (58) Kirchner, U.; Scheer, V.; Vogt, R. FTIR Spectroscopic Investigation of the Mechanism and Kinetics of the Heterogeneous Reactions of NO₂ and HNO₃ with Soot. *J. Phys. Chem. A* **2000**, *104*, 8908–8915.
- (59) Brown, J. F. The Infrared Spectra of Nitro and Other Oxidized Nitrogen Compounds. *J. Am. Chem. Soc.* **1955**, *77*, 6341–6351.
- (60) Pavia, D. L. *Introduction to Spectroscopy: A guide for Students of Organic Chemistry*; Harcourt College Publishers, 2001.
- (61) Klučáková, M.; Kolajová, R. Dissociation ability of humic acids: Spectroscopic determination of pKa and comparison with multi-step mechanism. *React. Funct. Polym.* **2014**, *78*, 1–6.
- (62) Klučáková, M.; Pekař, M. Behaviour of partially soluble humic acids in aqueous suspension. *Colloids Surf., A* **2008**, *318*, 106–110.
- (63) Wang, X.; Gemayel, R.; Hayeck, N.; Perrier, S.; Charbonnel, N.; Xu, C.; Chen, H.; Zhu, C.; Zhang, L.; Wang, L.; Nizkorodov, S. A.; Wang, X.; Wang, Z.; Wang, T.; Mellouki, A.; Riva, M.; Chen, J.; George, C. Atmospheric Photosensitization: A New Pathway for Sulfate Formation. *Environ. Sci. Technol.* **2020**, *54*, 3114–3120.
- (64) Patiño, P.; Méndez, M.; Pastrán, J.; Gambús, G.; Navea, J.; Escobar, O.; Castro, A. Oxidation of Cycloalkanes and Diesel Fuels by Means of Oxygen Low Pressure Plasmas. *Energy Fuels* **2002**, *16*, 1470–1475.
- (65) Gambús, G.; Patiño, P.; Méndez, B.; Sifontes, A.; Navea, J.; Martín, P.; Taylor, P. Oxidation of Long Chain Hydrocarbons by Means of Low-Pressure Plasmas. *Energy Fuels* **2001**, *15*, 881–886.
- (66) Atkinson, R.; Baulch, D. L.; Cox, R. A.; Crowley, J. N.; Hampson, R. F.; Hynes, R. G.; Jenkin, M. E.; Rossi, M. J.; Troe, J. Evaluated kinetic and photochemical data for atmospheric chemistry: Volume III – gas phase reactions of inorganic halogens. *Atmos. Chem. Phys.* **2007**, *7*, 981–1191.
- (67) Grimley, A. J.; Houston, P. L. The photochemistry of nitrosyl halides: The X+NOX→X₂+NO(v) reaction (X = Cl, Br). *J. Chem. Phys.* **1980**, *72*, 1471–1475.
- (68) Goodeve, C. F.; Katz, S.; Sugden, S. The absorption spectrum of nitrosyl chloride. *Proc. R. Soc. Lond., Ser. A: Math. Phys. Sci.* **1939**, *172*, 432–444.
- (69) Neuwirth, O. S. The Photolysis of Nitrosyl Chloride and the Storage of Solar Energy. *J. Phys. Chem. A* **1959**, *63*, 17–19.
- (70) Kistiakowsky, G. B. Photochemical decomposition of nitrosyl chloride. *J. Am. Chem. Soc.* **1930**, *52*, 102–108.
- (71) Gingerysty, N. J.; Osthoff, H. D. A compact, high-purity source of HONO validated by Fourier transform infrared and thermal-dissociation cavity ring-down spectroscopy. *Atmos. Meas. Tech.* **2020**, *13*, 4159–4167.
- (72) Baergen, A. M.; Donaldson, D. J. Formation of reactive nitrogen oxides from urban grime photochemistry. *Atmos. Chem. Phys.* **2016**, *16*, 6355–6363.
- (73) Liu, J.; Deng, H.; Zhang, R.; Zhang, R.; Song, W.; Li, X.; Luo, Y.; Wang, X.; Sasho, G. Physical and chemical characterization of urban grime: An impact on the NO₂ uptake coefficient and N-containing product compounds. *Sci. Total Environ.* **2022**, *838*, No. 155973.
- (74) Pandit, S.; Mora Garcia, S. L.; Grassian, V. H. HONO Production from Gypsum Surfaces Following Exposure to NO₂ and HNO₃: Roles of Relative Humidity and Light Source. *Environ. Sci. Technol.* **2021**, *55*, 9761–9772.
- (75) Liu, J.; Deng, H.; Li, S.; Jiang, H.; Mekic, M.; Zhou, W.; Wang, Y.; Loisel, G.; Wang, X.; Gligorovski, S. Light-enhanced heterogeneous conversion of NO₂ to HONO on solid films consisting of fluorene and fluorene/Na₂SO₄: an impact on urban and indoor atmosphere. *Environ. Sci. Technol.* **2020**, *54*, 11079–11086.
- (76) Deng, H.; Liu, J.; Wang, Y.; Song, W.; Wang, X.; Li, X.; Vione, D.; Gligorovski, S. “Effect of inorganic salts on N-containing organic compounds formed by heterogeneous reaction of NO₂ with oleic acid”. *Environ. Sci. Technol.* **2021**, *55*, 7831–7840.